Tesauro, M., Audet, P., Kaban, M. K., Bürgmann, R., Cloetingh, S. (2012): The effective elastic thickness of the continental lithosphere: Comparison between rheological and inverse approaches. - Geochemistry Geophysics Geosystems (G3), 13, 9

DOI: 10.1029/2012GC004162

Geochemistry Geophysics Geosystems G3

Article
Volume 13, Number 9
1 September 2012
Q09001, doi:10.1029/2012GC004162
ISSN: 1525-2027

Published by AGU and the Geochemical Society

The effective elastic thickness of the continental lithosphere: Comparison between rheological and inverse approaches

Magdala Tesauro
German Research Center for Geosciences, DE-14473 Potsdam, Germany (magdala@gfz-potsdam.de)

Pascal Audet
Department of Earth Sciences, University of Ottawa, Ottawa, Ontario K1N 6N5 Canada

Mikhail K. Kaban
German Research Center for Geosciences, DE-14473 Potsdam, Germany

Roland Bürgmann
Department of Earth and Planetary Science, University of California, Berkeley, California 94720, USA

Sierd Cloetingh
Department of Earth Sciences, Utrecht University, NE-3508 Utrecht, Netherlands

[1] Following the release of global continental effective elastic thickness (*Te*) maps obtained using different approaches, we now have the opportunity to provide better constraints on *Te*. We improve previous estimates of *Te* derived from thermo-rheological models of lithospheric strength (or Te_r) using new equations that consider variations of the Young's Modulus in the lithosphere. These new values are quantitatively compared with those obtained from an inverse approach (or Te_i) based on a comparison of the spectral coherence between topography and gravity anomalies with the flexural response of an equivalent elastic plate to loading. The two models show in general a good agreement, having equal means (at the 95% significance level) in about half of the continental areas. In other regions Te_i exceeds Te_r in about 65% of the data points, showing that Te_i provides an upper bound on *Te*. The two data sets have a similar range, but demonstrate different distributions. Te_r has a bimodal distribution, with the two peaks representative of the cratons and of the areas outside of them. In contrast, Te_i has more uniform distribution without predominant peaks. Our models show higher similarities in the Meso-Cenozoic orogens than in the Archaean and Proterozoic shields and platforms, due to the methods employed. For the regions with the most robust determinations of Te_r and Te_i, the relationship between them is close to linear. The results of this work can be used for further studies on the mechanical properties of the lithosphere.

Components: 9800 words, 8 figures, 1 table.

Keywords: coherence; continental lithosphere; effective elastic thickness; strength.

Index Terms: 8110 Tectonophysics: Continental tectonics: general (0905); 8138 Tectonophysics: Lithospheric flexure; 8159 Tectonophysics: Rheology: crust and lithosphere (8031).

Received 26 March 2012; **Revised** 31 July 2012; **Accepted** 1 August 2012; **Published** 1 September 2012.

Tesauro, M., P. Audet, M. K. Kaban, R. Bürgmann, and S. Cloetingh (2012), The effective elastic thickness of the continental lithosphere: Comparison between rheological and inverse approaches, *Geochem. Geophys. Geosyst.*, *13*, Q09001, doi:10.1029/2012GC004162.

1. Introduction

[2] The effective elastic thickness (*Te*) of the lithosphere is the thickness of an elastic layer that would respond to applied loads in the same way as the heterogeneous lithospheric plate. *Te* primarily depends on thermal gradient, composition and flexural plate curvature [e.g., *Burov and Diament*, 1996]. Any one of these values can be estimated if the others are known. Differences in the mechanical behavior of the oceanic lithosphere and continents can be explained by the control of different parameters: thermal gradient has a major control in the oceans, whereas in the continents crustal thickness and composition are also equally important. Therefore, the continental *Te* cannot be associated with a unique mechanical layer and does not correspond to any particular geotherm [e.g., *Burov and Diament*, 1995]. Indeed, continental *Te* estimates show large variations in plates of the same thermotectonic age [*Burov and Diament*, 1996]. In general, old tectonic provinces (>1.5 Gy) have a lithosphere that is colder and thicker, more depleted in basaltic constituents and, consequently, more dehydrated than younger ones [e.g., *Jordan*, 1978]. The combination of these factors is thought to make continental cratonic interiors more resistant to subsequent deformation [e.g., *Hirth and Kohlstedt*, 1996]. On the other hand, there exist other factors acting against strengthening due to cooling. For instance, in the active orogenic belts the lithosphere becomes weaker with time due to thickening of the crust and to the effects of flexural stresses, caused by bending of the lithosphere due to topographic and horizontal tectonic loads. Indeed, when a plate having a thick crust is loaded and flexed, the lower crust becomes sufficiently hot to significantly reduce its strength. This process results in mechanical decoupling between the upper crust and the mantle lithosphere and in large reduction of *Te* [e.g., *Burov and Diament*, 1996]. Other effects, such as reheating and hydrating of lithospheric mantle, occurring in the continental mobile mountain belts located in back-arc regions, can also decrease the continental *Te* [e.g., *Hyndman et al.*, 2005]. Furthermore, the horizontal stress due to extensional forces can weaken the lower crust and lead to subsequent crust-mantle decoupling, thus reducing the *Te* of ~400 Myr lithosphere by 15–20 per cent [*Cloetingh and Burov*, 1996; *Burov*, 2011].

[3] Recent maps of *Te* for large continental areas [e.g., *Audet and Bürgmann*, 2011; *Flück et al.*, 2003; *Pérez-Gussinyé and Watts*, 2005; *Pérez-Gussinyé et al.*, 2007, 2009; *Simons et al.*, 2003; *Swain and Kirby*, 2006; *Tassara et al.*, 2007; *Tesauro et al.*, 2009, 2012; *Wang and Mareshal*, 1999] show high values (>60 km) located within older provinces where the lithospheric thickness is much greater than in the younger provinces. Because of the correlation between large *Te* and thick lithosphere, *Te* maps of continents may be used to better understand their mechanical properties and to detect the lateral variability in lithospheric structure. Furthermore, since *Te* is directly related to lithospheric strength, it has been commonly used to understand the relationship between tectonic styles and lithospheric rheology in various tectonic settings. For example, *Watts et al.* [1995] examined the relationship between the style of fold-and-thrust belt tectonics and the rigidity of foreland lithosphere, while other studies [e.g., *Whitehouse et al.*, 2006] investigated vertical motions in response to loading or unloading during sedimentation, erosion and glaciation.

[4] Continental *Te* is typically estimated indirectly using a cross-spectral analysis of gravity and topography data [e.g., *Forsyth*, 1985]. However, these determinations may be biased by several factors and simplified assumptions, such as that of a homogeneous and continuous plate, and thus often provide inconsistent estimates of *Te* [e.g., *Artemjev and Kaban*, 1991]. In particular, *Te* estimates for cratons based on the transfer function (admittance) between the free air gravity and topography are in some cases significantly lower than values obtained from coherence analysis between Bouguer gravity anomalies and topography [e.g., *McKenzie*, 2003]. As a consequence, the role of the lithospheric mantle in controlling *Te*, and thus whether or not the strength resides entirely in the crust, has been a subject of controversy in the literature [see *Kirby and Swain*, 2009]. Furthermore, post-seismic deformation and field studies suggest that, at short time scales, the lower crust and upper mantle may readily deform, indicating low strength at those depths [*Bürgmann and Dresen*, 2008]. However, notwithstanding these issues, *Pérez-Gussinyé and Watts* [2005] and *Kirby and Swain* [2009] have shown that part of the discrepancy in the *Te* estimates can be attributed to the higher sensitivity of the admittance to un-modeled

subsurface loads. When both admittance and coherence method are formulated in a consistent manner, the results indicate that *Te* in cratons can be >100 km.

[5] *Audet and Bürgmann* [2011] presented a global map of *Te* over the continents calculated from a comparison of the spectral coherence between topography and gravity anomalies with that produced by the flexural response of an equivalent elastic plate to loading. The coherence method is less sensitive than the admittance to large variations in the ratio between subsurface and surface loads and is therefore more robust in the presence of subsurface loading [*Forsyth*, 1985]. In their study they use a wavelet transform to calculate the coherence, thereby improving the spatial resolution of *Te*. In the study of *Tesauro et al.* [2012] *Te* was determined on a global scale using the approach based directly on the strength distribution estimated from thermo-rheological parameters.

[6] In this work the *Te* of the continental areas is re-estimated by improving this approach. *Burov and Diament* [1995] suggested a method to estimate *Te* for several lithospheric layers with constant Young's Modulus (*E*). However, the lithosphere is strongly layered mechanically and the average *E* of the lithospheric mantle is almost double than of the crust. To compare the estimates with those obtained using the spectral coherence approach, we derive new equations to calculate *Te* from the lithospheric strength distribution considering different *E* for each lithospheric layer. We compare the new estimates with those of *Audet and Bürgmann* [2011]. This study thus presents for the first time a global comparison of *Te* from two independent, high-resolution techniques. These comparisons allow us to constrain the possible range of *Te* of the main geological provinces, as well as discuss differences and similarities observed in areas characterized by the crustal ages and structures. A discussion on potential uncertainties of the *Te* estimates emphasizes where future work is needed in order to provide more accurate constraints on the rheology of continental lithosphere.

2. Rheological *Te* Estimated From Lithospheric Strength

[7] As mentioned in the introduction, *Te* in the study of *Tesauro et al.* [2012] was determined from a distribution of the lithospheric strength. To estimate the latter we used new high-resolution compilations of crustal parameters. For example, the global map of sediments is obtained merging new compilations for the continents [*Tesauro et al.*, 2008; *Mooney and Kaban*, 2010] and oceans [*Divins*, 2003], whereas the Moho map, based on the global model CRUST 2.0 [*Bassin et al.*, 2000], is augmented in North America, Eurasia and Australia by the recent compilations of *Tesauro et al.* [2008], *Mooney and Kaban* [2010] and *Collins et al.* [2003].

[8] Different rheologies were assumed for the upper and lower continental crust, according to the age of the geological provinces [*Mooney*, 2009] and the seismic velocity of the constituent rocks. In doing so, we associate a "hard" rheology represented by granite-mafic granulite to Archean and old Proterozoic structures, a "soft" rheology represented by quartzite-diorite to Meso-Cenozoic structures and an "average" rheology represented by granite-diabase and quartzite-diabase to structures of intermediate age. The increase in stiffness of the rocks' rheology with age is exemplified by the metamorphic transition of the lowermost part of the crust from gabbro to eclogite through garnet granulite often found in the cratonic areas. The rherological classification made in *Tesauro et al.* [2012] on a global scale does not consider possible exceptions to this rheology-age dependency observed in some geological features. For instance, the Archean Wyoming province crust is very rich in quartz, while the Phanerozoic Siletzia and Great Valley blocks are extremely mafic [*Lowry and Pérez-Gussinyé*, 2011]. Nevertheless, the age-based crustal rheology affects *Te* estimates in cratons only marginally due to the dominant effect of cold geotherms (and thus stiff lower crust). A uniform dry olivine rheology was assumed for the mantle lithosphere. Rheological model parameters and strength equations are displayed in Table 1. We used the creep parameters obtained from experiments carried out on natural samples [e.g., *Goetze and Evans*, 1979; *Carter and Tsenn*, 1987; *Wilks and Carter*, 1990]. New laboratory measurements (see *Bürgmann and Dresen* [2008] for a review) have more control on the uncertainties in the rheological parameters. At the same time, these experiments utilize simple monophase synthetic minerals having a homogeneous grain size, which are designed specifically not to have the impurities usually present in the natural samples. Those impurities may be a primary source of the dislocations exploited by dislocation creep in natural rocks. Therefore, the extensions of the results of these experiments to real aggregate compositions remain to be demonstrated. Actually, the results of the new experiments compared to the old ones give higher values of the strength, probably because

Table 1. Rheological Model Parameters and Strength Equations[a]

Parameter	Symbol	Units	Sediments	Upper Crust	Lower Crust	Upper Mantle
Composition	-	-	-	Quarzite (dry)[1]/ Granite(dry)[1]	Mafic-Ganulite[2]/Diorite (wet) [1]/ Diabase (dry)[1]	Olivine (dry) [3]
Density min-max/mean	ρ	kg/m^3	1700–2776/2346	2617–2862/2804	2886–3122/3037	3312–3380/3352
Layer Thickness min-max/mean	z	km	0–21.5/2	1.5–51.5/24	0.5–32/9.5	5–254/118
Friction Coefficient ext/com	f	-	0.75/3	0.75/3	0.75/3	0.75/3
Pore fluid factor	λ	-	0.36	0.36	0.36	0.36
Power law exponent	n	-	-	2.72/3.3	4.2/2.4/3.05	3
Power law activation energy	Ep	$KJ\ mol^{-1}$	-	134/186	445/212/276	510
Power law strain-rate	A_p	$Pa^{-n}\ s^{-1}$	-	6.03×10^{-24}/ 3.16×10^{-26}	8.83×10^{-22}/1.26×10^{-16}/ 6.31×10^{-20}	7.0×10^{-14}
Dorn law activation energy	E_D	$KJ\ mol^{-1}$	-	-	-	535
Dorn law strain-rate	A_D	s^{-1}	-	-	-	5.70×10^{11}
Dorn law stress	σ_D	Pa	-	-	-	8.5×10^{9}
Strain rate	ε	s^{-1}	-	10^{-15}	10^{-15}	10^{-15}
Brittle Strength	$\sigma = f\rho gz(1-\lambda)$					
Creep Equations						
Power law creep	$\sigma = \left[\frac{\dot{\varepsilon}}{A_P}\right]^{\frac{1}{n}} . \exp\left[\frac{E_P}{nRT}\right]$					
Dorn law creep	$\sigma = \sigma_D \left(1 - \left[-\frac{RT}{E_D} . \ln\left(\frac{\dot{\varepsilon}}{A_D}\right)\right]^{1/2}\right)$					

[a]Numbers in square brackets indicate source: [1] *Carter and Tsenn* [1987]; [2] *Wilks and Carter* [1990]; [3] *Goetze and Evans* [1979].

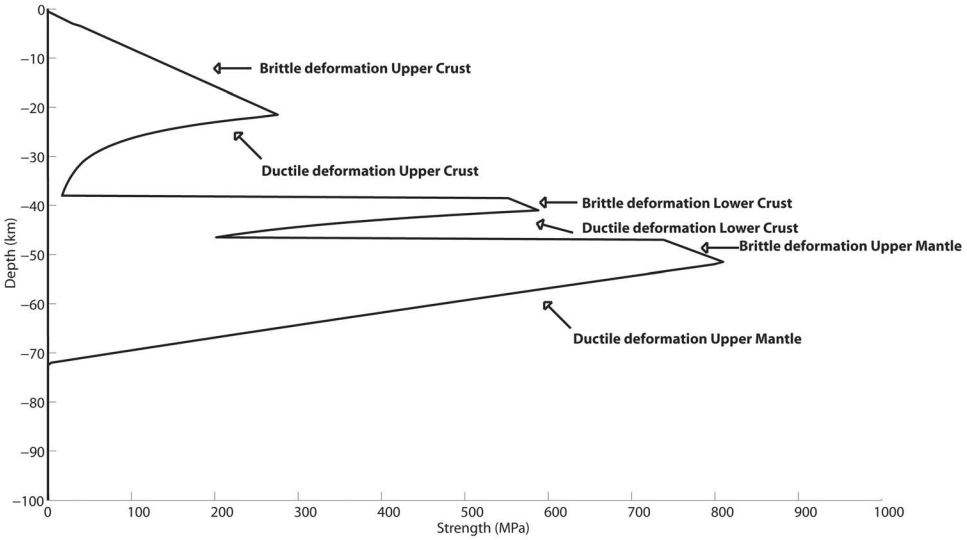

Figure 1. Example of a Yield Strength Envelope (YSE).

monophase rocks are stronger than polyphase ones [e.g., *Zhong and Watts*, 2010].

[9] We inferred the temperature distribution by combining the observed surface heat flow with seismic tomography data. The temperature distribution in the mantle lithosphere was obtained by inverting the seismic tomography model of *Ritsema et al.* [2004] following a mineral physics approach [*Cammarano et al.*, 2003]. Therefore, using these input parameters (see *Tesauro et al.* [2012] for further details on their values, the assumptions and laws used to estimate the lithospheric strength), we determined the Yield Strength Envelope (YSE) which describes the distribution of strength with depth [*Goetze and Evans*, 1979] for each data point of the study area. The YSE, as shown in Figure 1, is represented by two different types of curves: the straight line, representing the brittle failure, shows an increase of strength with depth [*Byerlee*, 1978], while the curved line, representing the ductile deformation, shows that the strength decreases downward exponentially, on account of the increase of temperature [*Burov and Diament*, 1995].

[10] Several authors have described how to estimate the effective elastic thickness from the YSE [*Lowry and Smith*, 1995; *Burov and Diament*, 1995]. In this approach, the elastic stress profile, caused by bending of an ideal elastic plate with known curvature and Young's Modulus (E), is truncated by the YSE, thus lowering the total bending moment from which the effective rigidity is calculated. However, these calculations are difficult to perform due to poorly constrained curvature and complications caused by mechanical decoupling. By assuming that curvature is small, *Burov and Diament* [1995] have devised an approximate method by which the effective elastic thickness can be estimated as the sum of the mechanically competent layers composing the lithosphere, thus bypassing the need to calculate the bending moment. Following this approach, the mechanical thickness of each competent layer is defined by the depth to the top extending down to the depth at which the yield stress is lower than some pre-defined threshold value (e.g., 10 MPa used in *Ranalli* [1994]). The lithospheric layers are considered coupled or decoupled when the strength contrast across the layer decreases above or below this threshold, respectively. When the lithosphere consists of n competent layers decoupled from each other, *Te* is estimated as follows:

$$T_e^{(n)} = \left(\sum_{i=1}^{n} \Delta h_i^3 \right)^{1/3} \quad (1)$$

where Δh_i is the thickness of the i_{th} competent layer. In contrast, if the layers are mechanically coupled, the upper limit of *Te* is estimated as total thickness of the competent layers':

$$T_e^{(n)} = \sum_{i=1}^{n} \Delta h_i \quad (2)$$

These equations [*Burov and Diament*, 1995] do not directly include elastic effects (in particular, the Young's Modulus for each layer); however the validity of the equations depends on the use of uniform elastic parameters, and *Te* estimated from this approach is indirectly related to E via the elastic moduli obtained from the seismic models used in

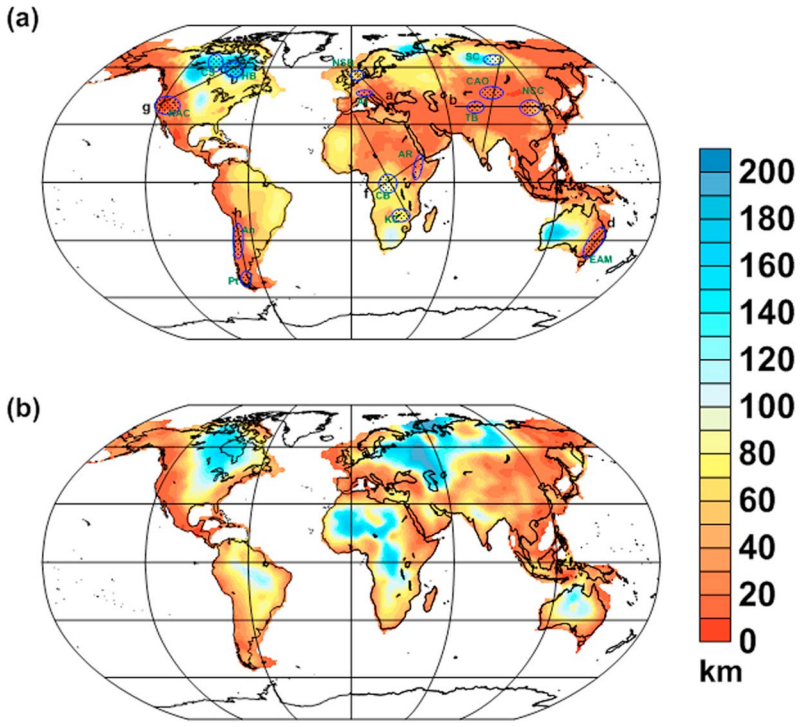

Figure 2. Global effective elastic plate thickness (*Te*) of the lithosphere (km) based on two different methods. (a) *Te* estimated from a rheological approach (Te_r), based on the lithospheric strength distribution [*Tesauro et al.*, 2012] and improved in this study. Black lines show cross-sections location displayed in Figures 5a–5h. The dotted areas delimited by blue contours correspond to selected regions, where correlation between Te_r and Te_i is estimated (Figure 8). Green acronyms are as follows: Al: Alps; An: Andes; CAO: Central Asian Orogen; CB: Congo Basin; CS: Canadian Shield; EAM: Eastern Australian Margin; EAR: East African Rift; HB: Hudson Basin; KC: Kalahari Craton; NAC: North American Cordillera; NCC: North China Craton; NSB: North Sea Basin; Pt: Patagonia; TB: Tarim Basin. (b) *Te* estimated from an inverse approach (Te_i) based on a comparison of the spectral coherence between topography and gravity anomalies and the flexural response of an equivalent elastic plate to loading [*Audet and Bürgmann*, 2011].

the calculation of the geotherms. In addition, the crust and mantle have significantly different values of *E*. In order to compare with the values obtained from the inverse approach where a single, uniform value of the Young's Modulus is used to estimate *Te* (E = 100 GPa, see below), we modify the approach of *Burov and Diament* [1995] and re-estimate *Te* taking into account depth variations in *E*.

[11] By definition, the effective elastic plate thickness is the thickness of a homogeneous plate, whose flexural rigidity $D_0 = \frac{E_0 Te_0^3}{12(1-\sigma_0^2)}$ is equal to the flexural rigidity of a welded heterogeneous plate $D_1 = \frac{E_1 Te_1^3}{12(1-\sigma_1^2)}$. Therefore, we obtain the following:

$$T_{e0} = \sqrt[3]{\frac{E_1}{E_0}} \mathrm{T_{e1}} \qquad (3)$$

where E_0 = 100 GPa is the reference value, E_1 is the Young's Modulus estimated as the Voigt (weighted) average of *E* of all coupled lithospheric layers [e.g., *Altenbach*, 2000]. Te_1 is total thickness of the coupled competent layers (equation (2)). In case of decoupling conditions, Te_1 is estimated according to equation (3) for each of the decoupled layers (or for two coupled layers and one decoupled) and then equation (1) can be directly applied with the modified values.

[12] Based on the assumed crustal rheology and on the experimental results of *Christensen* [1996], we assign E = 90 GPa to the upper crust and values of 99, 106 and 111 GPa to the lower crust, corresponding to rheologies of diorite, diabase and mafic granulite, respectively. We derived the Young's Modulus of the lithospheric mantle by estimating the bulk and shear modulus and the Poisson coefficient of peridotite, its most representative rock, through a mineral physics approach [e.g., *Cammarano et al.*, 2003]. We found that the Young's Modulus of the lithospheric mantle is nearly double that of the crustal rocks. Despite the

dependence of E on composition, as well as on pressure and temperature variations, these factors have a small effect on E (<10 GPa) in the range of brittle conditions. This uncertainty influences Te_0 insignificantly (on the order of about 1 km). Therefore, we assume a constant value of E (180 GPa) for the lithospheric mantle. The new *Te* estimates are displayed in Figure 2a. We refer to *Te* estimates obtained using this approach as the 'rheological *Te*', or Te_r.

2.1. Inverse *Te* Estimated From Gravity and Topography

[13] The inverse approach consists of estimating *Te* from the statistical relationships between gravity anomalies and the topography. The underlying principle of this approach is based on the concept of flexural isostasy, where large vertical loads are compensated by the flexure of a thin elastic plate. The parameter controlling the vertical displacement of the plate is the flexural rigidity D, which is a function of both the Young's Modulus (E) and the plate thickness (*Te*),

$$D = \frac{ET_e^3}{12(1-\sigma^2)} \quad (4)$$

where σ is Poisson's ratio, taken to be 0.25. Due to the stronger dependence of D on *Te* compared to E, spatial variations in rigidity are mapped into variations in thickness of the elastic plate using a constant value for the Young's Modulus (E = 100 GPa). Vertical loads can be emplaced on the surface (e.g., topographic loading) or from below (e.g., underplating) and compensation results in the observed topography and the deflection of an internal surface at the depth of compensation. This surface is normally taken to be the crust-mantle boundary, and deflections can be estimated from the downward continuation of gravity anomalies. The spectral relationships between gravity anomalies and the topography thus contain important information on the state of compensation of vertical loads, and two approaches have been traditionally used to obtain estimates of *Te*: the inversion of the admittance using free-air gravity anomalies or the inversion of the coherence using Bouguer gravity anomalies.

[14] The traditional approach in the continents is to approximate the Earth's isostatic response as a linear filter between gravity anomalies and topography, thus allowing the use of the convolution theorem to calculate the isostatic response function [*Lewis and Dorman*, 1970]. Deconvolution of gravity and topography in the spectral domain is performed by spectral division (i.e., calculating the admittance function), which removes the undesired effect of noise in the gravity data. The admittance is then modeled by solving the equation for the flexure of a uniform elastic plate with either or both surface and subsurface loading. Following the work of *Lewis and Dorman* [1970], most studies have used free-air gravity anomalies in the calculation of the admittance. However, as demonstrated by *Forsyth* [1985], the admittance method is extremely sensitive to the relative amplitude of initial subsurface and surface loading.

[15] The coherence method, developed by *Forsyth* [1985], is sensitive to different properties of the load compensation mechanism. At long wavelengths the plate is likely to be fully deflected and the topography and Bouguer gravity are expected to be inversely correlated. At smaller wavelengths the elastic plate is able to support the loads elastically and the topography and Bouguer gravity may have statistically random phase differences. The statistics of the phase relationship as a function of wavelength can thus provide an estimate of the effective plate rigidity. This method is less sensitive to the final amplitude of the loads than the admittance function, and is thus more robust in the presence of subsurface loading.

[16] A problem common to both techniques is their instability in the presence of flat topography that can introduce noise in the spectral functions and thus blur the structural information. As *Kirby and Swain* [2009] have pointed out, this problem can give rise to significantly different *Te* values whether one uses the admittance or the coherence function in the inversion. Furthermore, *Kirby and Swain* [2009] further showed that robustness of *Te* estimates from the Bouguer coherence method can be evaluated by the value of the imaginary component of the complex coherency function at the wavelength of flexure, where a value greater than 0.4 implies bias. In addition, because the estimation is performed in the spectral domain, all spatial information is lost and the resolution of *Te* values is low, depending on the size of windows used in the estimation. Several spectral techniques have been developed in the past ~20 years to improve the spatial resolution of *Te* estimates. Recent models of continental *Te* using spectral methods are consistent and show significant variations at all scales.

[17] Here we use the most recent global *Te* model of *Audet and Bürgmann* [2011] that was obtained using the continuous wavelet transform to calculate the coherence between Bouguer gravity anomalies and the topography. The wavelet transform affords

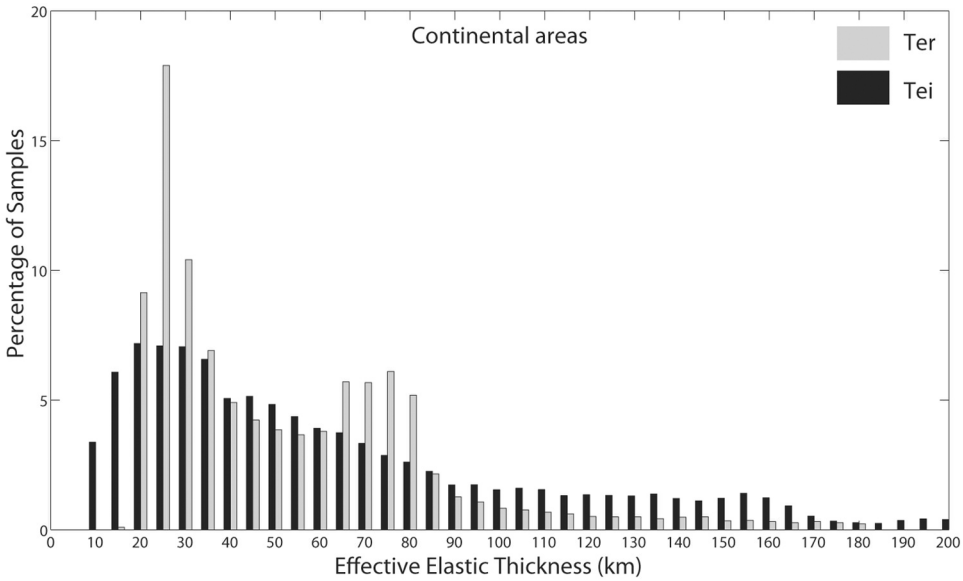

Figure 3. Histograms showing Te_r (in gray) and Te_i (in black) distributions in continental areas.

optimal resolution in both spatial and spectral domains that allows us to estimate *Te* at each grid point. In this approach estimates of *Te* are obtained by minimizing the least squares misfit between the observed coherence between Bouguer gravity and topography with the coherence predicted by the flexure of a thin isotropic elastic plate under surface and internal loading. We use the $1' \times 1'$ SRTM bathymetry/topography model of *Smith and Sandwell* [1997] (http://topex.ucsd.edu/) and the gravity model EGM2008 [*Pavlis et al.*, 2008]. For each continent we extract the gravity and topography data on transverse Mercator (rectangular) grids and convert free-air gravity anomalies to Bouguer anomalies. After inversion the *Te* estimates are back-projected onto a $10' \times 10'$ grid. Estimates that are biased by gravitational noise (see above discussion and *Kirby and Swain* [2009] and *Audet and Bürgmann* [2011]) are excluded from the analysis. The final map is shown in Figure 2b. We refer to *Te* estimates obtained using this approach as 'inverse *Te*', or Te_i.

3. Comparison of the *Te* Estimates Using the Rheological and Inverse Approach

[18] *Te* in the continental areas is primarily related to the combined effects of rheological and thermal heterogeneity that control the mechanical coupling or decoupling conditions of the lithospheric layers. Large variations in *Te* estimated from both the rheological and inverse approaches (Figures 2a and 2b) occur across sutures that separate provinces with major differences in strength [*Audet and Bürgmann*, 2011; *Tesauro et al.*, 2012]. For example, crust–mantle decoupling drastically reduces the total integrated strength and *Te* (change of ~40 km or greater) of the lithosphere over the narrow (~100 km) transition from the interior of the North and South American plates to the Cordillera.

[19] Te_r in the continents (Figure 3) ranges from 15 to 180 km and shows a bimodal distribution. The main peak (~18% of data) is at ~25 km, a representative value for the areas outside of cratons, while some smaller peaks (>25% of data) between 65 and 80 km are common values for the cratons [e.g., *Watts*, 2001]. This clustering results from the vertical distribution of strength: depending on the ductile strength of the lower crust, the upper continental crust is mechanically coupled or decoupled from the mantle, resulting in very different *Te* values. In contrast, Te_i (Figure 3) spans a larger range (from 10 to 200 km) and is not distributed around a predominant peak. However, ~25% of data points show Te_i between 20 and 35 km, which are boundary values of a typical range of *Te* in the areas outside of cratons [e.g., *Watts*, 2001]. The cratons do not seem to be represented by a common value or range of Te_i. Nevertheless, there is a significantly greater proportion of $Te_i > 100$ km in the cratons compared to Te_r (20% vs 7%).

[20] To examine the consistency of the two data sets, we performed a Welch's t-test within 15° circular moving windows, testing the null hypothesis

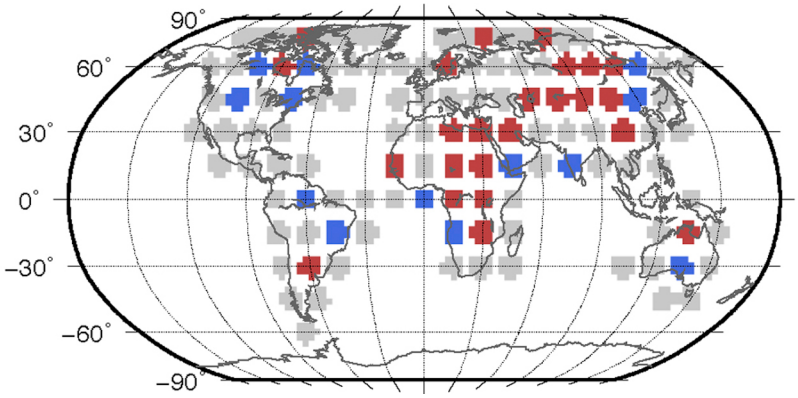

Figure 4. Results of Welch's t-test performed within 15° circular moving windows, testing the null hypothesis that the means of the two distributions are equal given their unequal variance. Areas in gray indicate regions where we cannot reject the null hypothesis at the 95% significance level; blue and red areas indicate regions where we can reject the null hypothesis. Blue areas show regions for which $Te_r > Te_i$; red areas indicate $Ter < Te_i$.

that the means of the two distributions are equal given their unequal variance. In this test we assume 20% uncertainty on individual estimates for both Te_r and Te_i in the calculation of the distribution variance. The results (Figure 4) show that in about half of the continental areas the two distributions have equal means (at the 95% significance level), while in the other parts, such condition is not found. It is worth noting that regions where the means are equal are found mainly on continental margins and where topography is high. This is also where Te_i estimates are most robust and free of gravitational noise bias [*Audet and Bürgmann*, 2011]. In the cases where we can reject the null hypothesis we also plot the sign of the difference between averages. We find that $Te_i > Te_r$ in about 65% of data points, suggesting that Te_i provides an upper bound on *Te*. This generally occurs in low-elevation areas including Shield and Platform provinces. The quality of the agreement between the two data sets is also visible in more detail from the cross-sections displayed in Figures 5a–5h). We can observe that, although Te_i appears generally smoother than Te_r, which is likely due to the smoothing effect of the spectral estimation technique in the case of Te_i, the large-scale patterns coincide. The two data sets show very similar values in the Paleozoic and Meso-Cenozoic orogens, like in the Dinarides (Figure 5a), in the Central Asian Orogen (Figures 5b and 5c), in the Eastern Australian margin (Figure 5d) and in the southern part of the Andes (Figure 5h). In other areas, like in the Siberian Craton (Figure 5c) and in the Congo Basin (Figure 5f), they are characterized by similar trends, with a shift in the values up to ∼50 km. In few cases Te_r and Te_i have opposite trend, like in the North Sea (Figure 5a) and in part of the North American craton (Figure 5g). A major disagreement is found in the African continent (Figure 5e), in particular in the African metacraton, also revealed by the Welch's t-test. Nevertheless, it is still possible to identify similarities in the shape of both trends (e.g., change in *Te* gradient). In order to investigate the consistency of the two data sets in more detail, we analyze their distributions for different crustal ages and tectonic provinces. In doing so, we divide the continental areas into four major age groups (Archean, Proterozoic, Paleozoic and Meso-Cenozoic) and tectonic provinces (Shield and Platform, Orogen, Basin and Extended crust and Large Igneous provinces), using recent compilations of these parameters [e.g., *Mooney*, 2009]. We display the distributions of Te_r and Te_i for the crustal units of the above mentioned age groups and tectonic provinces, which are represented by more than 1000 data points (Figure 6): Archean Shield and Platform provinces, Proterozoic Shield and Platform provinces, Proterozoic Basins and Extended crust provinces, Paleozoic Orogens provinces, Paleozoic Extended crust and Basin provinces, Meso-Cenozoic Orogens provinces and Meso-Cenozoic Extended crust and Basin provinces.

[21] In the Shield and Platform provinces of Archean age (Figure 7a), corresponding to part of the cratons, both data sets have >25% of *Te* values between 65 and 85 km, which are typical estimates of areas characterized by cold and thick lithosphere [e.g., *Watts*, 2001]. A smaller peak (∼15% of data) occurring between 150 and 160 km is present only in the Te_i data set. However, in some specific Archean regions, such as the Canadian Shield and the Hudson Basin (Figures 2a and 2b), both models show very large values (from 150 to 180 km), which are also found in previous studies [e.g., *Flück et al.*, 2003;

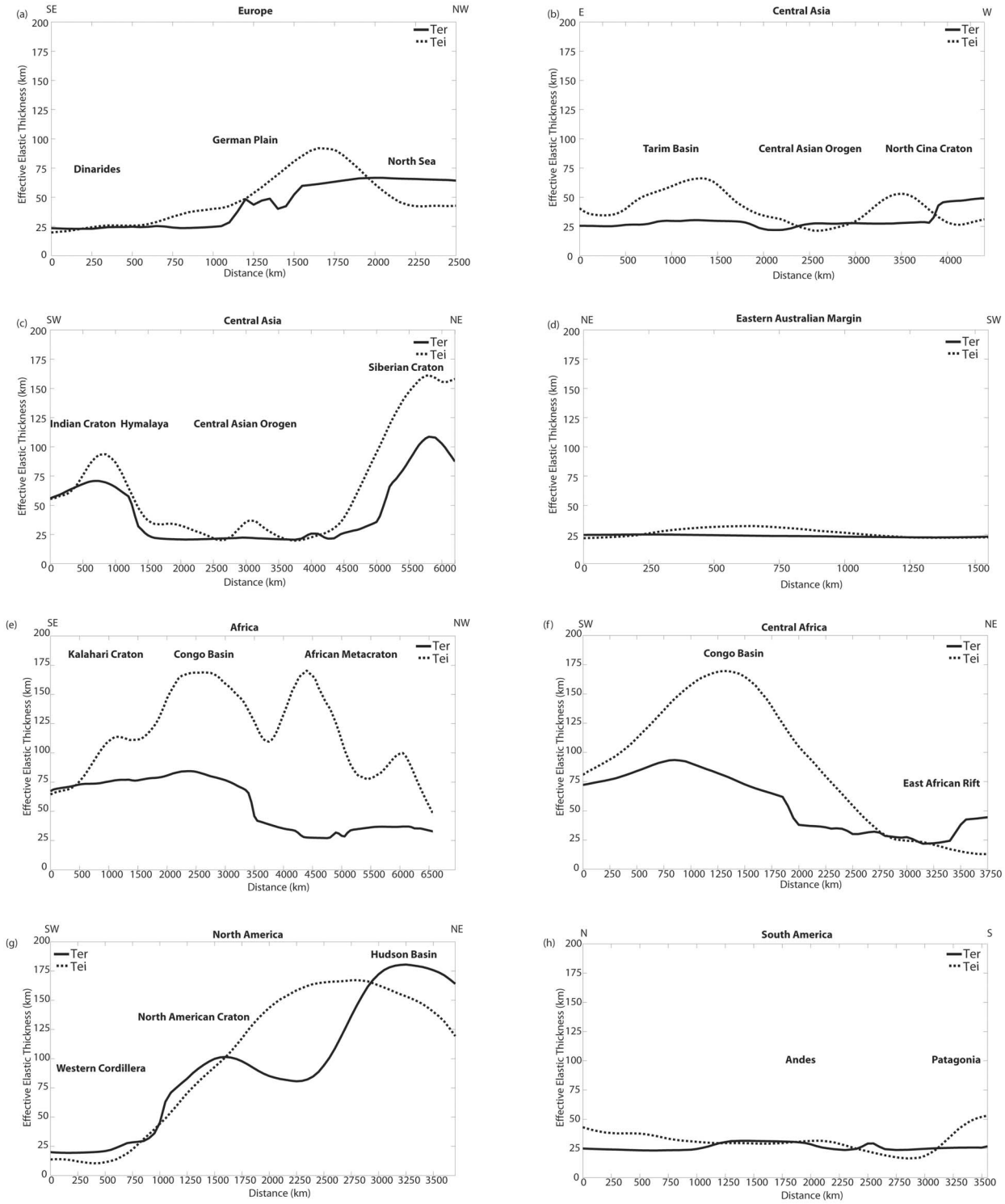

Figure 5. (a–h) Te_r (solid lines) and Te_i (dotted lines) estimated along cross-sections through the main geological features. See Figure 2a for cross-sections location.

Kirby and Swain, 2009]. In other regions, such as the Kalahari craton, the agreement between the two data sets is good and both models show *Te* prevalently between 65 and 75 km. Similar values were also inferred from previous coherence studies [e.g., *Pérez-Gussinyé et al.*, 2009]. In the Siberian Craton Te_r ranges between 110 and 145 km, while the range

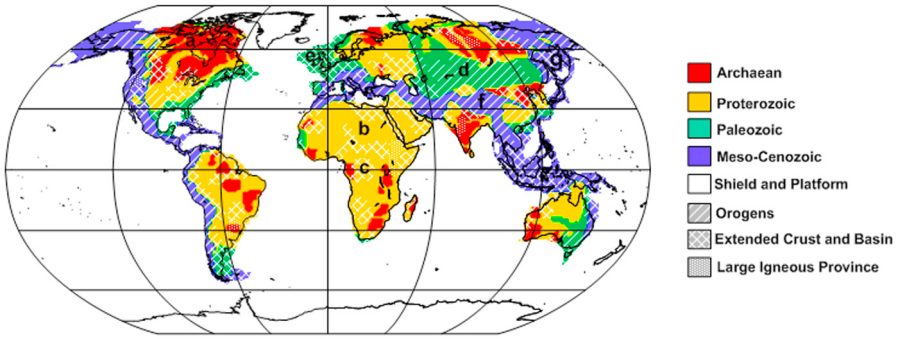

Figure 6. Map of crustal ages and tectonic provinces, modified after *Mooney* [2009]. Letters show the location of the crustal units considered in this study, obtained from the overlap between the two maps, as follows: a, Archean Shield and Platform provinces; b, Proterozoic Shield and Platform provinces; c, Proterozoic Extended crust and Basin provinces; d, Paleozoic Orogens provinces; e, Paleozoic Extended crust and Basin provinces; f, Meso-Cenozoic Orogens provinces; g, Meso-Cenozoic Extended crust and Basin provinces.

of Te_i is slightly larger (most of values are between 95 and 160 km).

[22] In the Shield and Platform provinces of Proterozoic age (Figure 7b) Te_r shows a main peak (∼40% of data) between 65 and 80 km and a smaller one (∼25% of data) between 25 and 40 km, whereas the Te_i values are broadly distributed over the entire range (from 10 to 200 km), without showing a dominant peak. The largest values (>100 km) are predominant in the Te_i compared to the Te_r model (41% vs 12% of data), whereas the lowest values (<30 km) are present in a small proportion in both data sets (<10% of data). These results suggest that these provinces are characterized by a cold and thick lithosphere, where the layers are coupled (e.g., the Proterozoic North American craton) and in a smaller proportion by regions with higher lithospheric temperatures, where the lithospheric layers are decoupled (e.g., part of the African metacraton).

[23] Te_r in Basins and Extended crust provinces of Proterozoic age (Figure 7c) shows a high peak (14% of data) at 30 km and a lower one (10% of data) around 65 km, while most of Te_i values span the range 25–75 km. The largest values (>100 km) are observed prevalently in Te_i (19% vs 3%), while the lowest (<30 km) are present in both models in equal proportion (∼14%). Therefore, in these areas the decoupling conditions seem to dominate over those of coupling. Looking at some specific geological features, we can observe that in the Tarim basin Te_r is ∼30 km, a relatively low value, which suggests the presence of decoupling conditions, whereas Te_i is about twice as large. In contrast, in the Congo Basin both models show large *Te* estimates (>80 km), even though Te_i is still about twice as large as Te_r. A flexural and a coherence study in the Tarim and Congo basin [*Teng*, 1991; *Pérez-Gussinyé et al.*, 2009] finds values of *Te* intermediate with respect to those of our models (∼45 km and ∼100 km, respectively).

[24] In Orogens provinces of Paleozoic age (Figure 7d) the two models show predominant peaks around similar values: Te_r (>25% of data) at 25 km, and Te_i (∼12% of data) at 20 km. Furthermore, both data sets have a high percentage (>35% of data) of low values (<30 km). In contrast, estimates larger than 100 km represent 10% of the Te_i data and are almost absent (only 2% of data) in the Te_r model. There is also a very good agreement between the two models in specific geological features, such as the Central Asian Orogen, where predominant values of Te_r and *Tei* are around 20 and 25 km, respectively.

[25] In Basin and Extended crust provinces of Paleozoic age (Figure 7e), Te_r spans a relatively large range (mostly between 25 and 80 km), but with a higher percentage of values over 50 km. On the other hand, Te_i spans a similar range, but with a prevalence of values lower than 45 km. Concerning specific geological features, the two models are in a good agreement in the North Sea, where both data sets find values around ∼60 km. On the other hand, in other areas like Patagonia, Te_i ranges mainly between 35 and 45 km, whereas Te_r values are half as large. In this area other coherence studies [e.g., *Tassara et al.*, 2007; *Pérez-Gussinyé et al.*, 2007] show values more similar to Te_r (between 20 and 30 km).

[26] In Orogens and Extended crust and Basin provinces of Meso-Cenozoic age (Figures 7f and 7g)

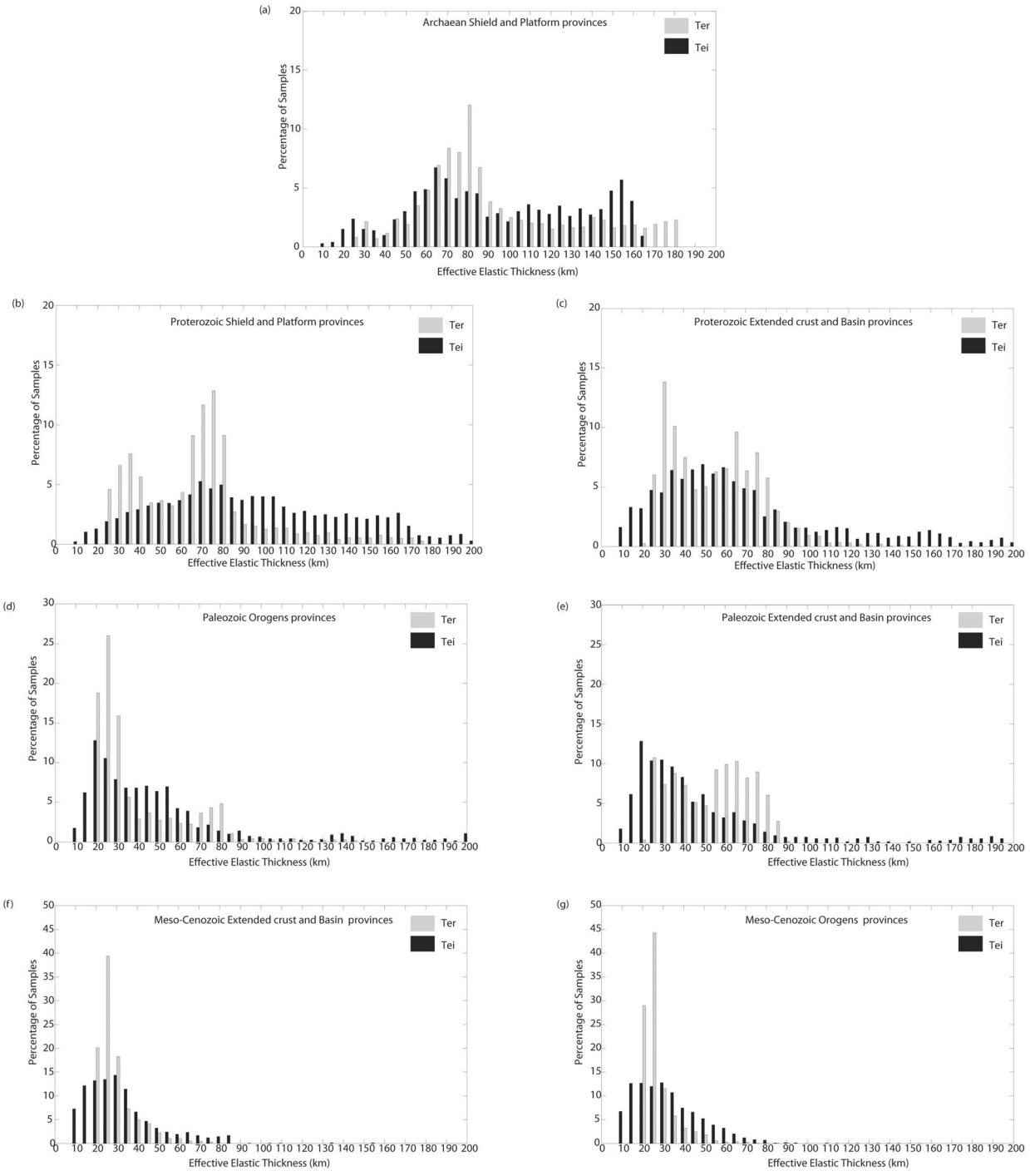

Figure 7. Histograms showing Te_r (in gray) and Te_i (in black) distributions for different crustal units, obtained from a range of age groups and tectonic provinces. (a) Archean Shield and Platform provinces; (b) Proterozoic Shield and Platform provinces; (c) Proterozoic Extended crust and Basin provinces; (d) Paleozoic Orogens provinces; (e) Paleozoic Extended crust and Basin provinces; (f) Meso-Cenozoic Orogens provinces; (g) Meso-Cenozoic Extended crust and Basin provinces.

the agreement between the two models is quite strong, both data sets are characterized by a high percentage (between 50% and 80%) of low values (<30 km) and by the absence of estimates larger than 100 km. Therefore, both data sets span a relative narrow range, with ~80% of data between 20 and 30 km (Te_r) and 10 and 45 km (Te_i), respectively. The agreement is also good in specific geological

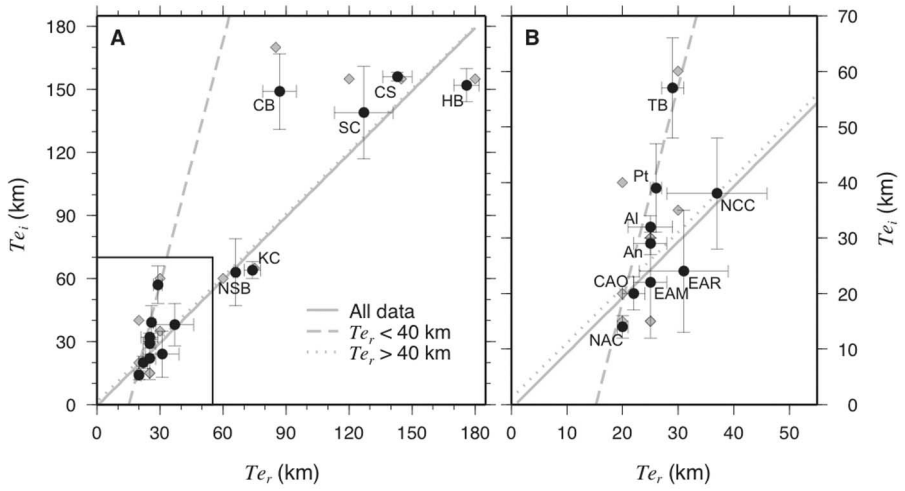

Figure 8. Correlation between rheological (Te_r) and inverse (Te_i) approaches for selected areas (see Figure 2a for their location). Black circles and error bars are mean and standard deviation for selected areas; gray diamonds are the modes. Gray lines are linear regressions for all data (solid line: slope of 1.00 ± 0.04, intercept of −1 ± 2 km, r = 0.94) and subsets of data (Te_r > 40 km, dotted line: slope of 1.0 ± 0.1, intercept of 1 ± 10 km, r = 0.89; and Te_r < 40 km dashed line: slope of 3.9 ± 0.5, intercept of −59 ± 4 km, r = 0.92). Inset in Figure 8a is shown in Figure 8b. Acronyms are listed in the caption of Figure 2a.

features, where the difference between the two data sets is ∼5 km. In the North American Cordillera Te_r is around 20 km, whereas Te_i∼15 km. In contrast, in the Alps and the southern part of the Andes Te_i is slightly larger (∼30 km) than Te_r (∼25 km). Low *Te* values in these regions (in the range of 10–30 km) are also inferred from previous coherence [e.g., *Tassara et al.*, 2007; *Pérez-Gussinyé et al.*, 2007] and flexural studies [e.g., *Prezzi*, 1999; *Kruse and Royden*, 1994]. The largest difference between the two models is observed in the Eastern Australian margin, where predominant Te_r values (∼25 km) are 10 km larger than those of Te_i.

[27] We now examine in more detail which representative geological features have *Te* estimates consistently constrained by our models. In Figure 8 we plot the average and standard deviations of Te_r and Te_i within selected regions for which the Te_i results are most robust and have the lowest uncertainty. These regions have formed in various tectonic settings and ages and include Archean cratons (e.g., the Kalahari and Siberian craton), Proterozoic and Paleozoic basins (e.g., the Tarim and the North Sea Basin) and Paleozoic and Meso-Cenozoic orogens (e.g., the Central Asian Orogen and the Alps). Despite the relatively large differences between Te_r and Te_i found in a few cases, the relation between their average values in the selected regions is close to linear. In particular the slope of the linear regression is indistinguishable from unity and the intercept is close to zero. Dividing the results into two groups, one where Te_r < 40 km and the other where Te_r > 40 km, we can observe that for the latter the correlation is higher and the slope is unity. The line where Te_r < 40 km is steeper than the other one, showing average estimates of Te_i ∼1.5 time larger than those of Te_r. However, we note that one data point may have an undue effect on the regression (outlier), in which case the result would be in agreement with the regression for Te_r > 40 km. Furthermore, even if the average values of the two models show larger relative differences when Te_r is <40 km, the range of their estimates appears in a better agreement in the orogens, characterized by low *Te* values (Figures 2a and 2b). In these areas Te_i estimates are well constrained, due to high signal-to-noise ratio (i.e., high topography). Furthermore, Te_r values reflect the decoupling conditions of the lithospheric layers and the higher contribution to *Te* from the thick crust compared to that of the hot and weak mantle [*Tesauro et al.*, 2012]. Indeed, despite the large uncertainties of rheological parameters for the crust, if the lithospheric mantle is weak, the *Te* is mainly controlled by the stiffness of the crust and can therefore only slightly exceed the crustal thickness (on average ∼40 km [*Christensen and Mooney*, 1995]). Consequently, in these regions the range of *Te* is well constrained by both approaches. These results confirm the hypothesis of low *Te* values within orogens [e.g., *Watts and Burov*, 2003], which in some cases may be due to the strong ductile flow in the lower crust and of the sub-crustal mantle as a consequence of the loading of weak continental

lithosphere [e.g., *Tesauro et al.*, 2011]. In particular, lower crustal flow has been proposed to explain crustal thickening and surface uplift in the absence of upper crustal shortening beneath the eastern Tibetan plateau [*Clark and Royden*, 2000] and in the central Andes [e.g., *Ouimet and Cook*, 2010; *Yang et al.*, 2003]. Such flow will eventually lead to a flattening of the Moho and the collapse of topography [e.g., *Watts and Burov*, 2003].

[28] Concerning the relationship between *Te* and seismicity, previous studies [e.g., *Watts and Burov*, 2003; *Burov*, 2010] have found that *Te* differs usually in the continental areas from the seismogenic layer thickness (*Ts*). The former reflects the integrated brittle, elastic and ductile strength of the lithosphere, on geological time scale (>10^5 yrs), while the latter is indicative of the depth to which anelastic deformation occurs as unstable frictional sliding and reflects weakness on historical time scales in the most competent part of the crust. The studies of *McKenzie and Fairhead* [1997] and *Jackson* [2002] have used the free-air admittance method to estimate continental *Te* values lower than *Ts* (<40 km). However, such low values might be due to inadequate formulation of the mechanical (flexural) problem in these models [e.g., *Kirby and Swain*, 2009; *Burov*, 2010]. In the study of *Tesauro et al.* [2012] we showed that crustal seismicity is mainly localized in the Meso-Cenozoic provinces, where both *Te* models show prevalently low values (<30 km). However, the similarity of the range of *Te* and *Ts* in these areas does not demonstrate the existence of a relationship between these parameters. Low *Te* can be a consequence of all the geological processes that have affected these features through time [e.g., *Watts and Burov*, 2003]. Furthermore, also in these regions *Te* usually exceeds *Ts*. Indeed, most of the crustal seismicity (88%) occurs in the uppermost part of the crust [*Tesauro et al.* 2012] at a depth typically shallower than *Te*, which includes also a contribution from the aseismic part of the lithosphere.

4. Potential Uncertainties of the *Te* Estimates

[29] The reason for the discrepancy between Te_r and Te_i in the cold and stiff cratons and in some basins (e.g., the Tarim and the Congo basin) can be partly ascribed to their flat topography, which decreases the reliability of Te_i. However, as demonstrated by *Kirby and Swain* [2009], the effect of low topography tends to increase the estimate uncertainty rather than represent a bias toward largest estimates. Alternatively, it may indicate the limitations of rheological parameters and rheological laws that are applicable in this setting.

[30] In the strongly mechanically coupled cratons, the contribution of the competent crustal layers to Te_r is less significant than that of the lithospheric mantle. However, the maximum thickness of the mechanically strong part of the lithospheric mantle does not correspond to that of the lithosphere, but is much thinner. Uncertainties on the rheological law, creep parameters and geothermal regime prevent us from constraining the upper limit of this thickness. We estimated the ductile strength of the lithospheric mantle using the Dorn law, which describes the creep mechanism dominant at high stress (>200 MPa). The rheological parameters were only estimated using "dry" olivine rheology [*Goetze and Evans*, 1979], which limits the thickness of the competent lithospheric mantle to the depth of the ~750°C geotherm. Uncertainties in the values of the creep parameters and/or on the applicability of the rheological law (e.g., power law creep may be dominant at temperature >800°C) may extend the thickness of the competent mantle to the depth of a hotter isotherm (850~900°C). Consequently, the calculated Te_r in the areas characterized by dry mantle conditions and coupled lithospheric layers may in fact be underestimated by up to 20%.

[31] The uncertainties of the thermal model depend on those of the seismic tomography, of the elastic parameters and of the compositional and anelasticity model used [e.g., *Goes et al.*, 2000]. In *Tesauro et al.* [2012] we have shown that the maximum uncertainty of the *S*-wave velocity of the tomography model used for temperature inversion is ~0.05 km/s, which translates into errors in estimates of temperature up to ~150°C in the cold cratons. However, this uncertainty affects only the areas where data coverage is poor (e.g., Greenland and Antarctica), which are excluded in this study. In other low-temperature zones the uncertainty is likely reduced to half of the maximum value, causing errors in estimates of temperature up to ~70°C. The effect is significantly smaller in the hot areas, where velocity variations correspond to smaller temperature changes due to anelasticity. The largest uncertainties of the elastic parameters are those related to their temperature derivatives (10% and 20% [e.g., *Cammarano et al.*, 2003]), leading to uncertainty in the inferred temperatures of about ±70°C above 300 km [*Tesauro et al.*, 2010]. Temperature uncertainties due to composition mostly depend on the correct evaluation of the degree of depletion in iron component affecting the cratonic mantle. A variation in Mg#

(100 × Mg/(Mg + Fe)) by 4–5 units, which corresponds to a typical difference between Archean to Phanerozoic mantle, causes a change of mantle temperature by ∼200°C [e.g., *Lee*, 2003], if anelasticity is not activated (<900°C). Therefore, the compositional effect plays a more significant role in the cold Achaean cratons [e.g., *Hieronymus and Goes*, 2010]. In contrast, in tectonically active areas, the melting temperature is reached at shallow depths (about 100 km) and the effect of the compositional differences is strongly reduced. For these areas, the main uncertainty is due to the anelasticity model used [*Shapiro and Ritzwoller*, 2004]. To reduce the uncertainties related to the compositional variations, we used in *Tesauro et al.* [2012] compositions that are representative for the mantle lithosphere over large areas, such as On Craton as characterized by *McDonough and Rudnick* [1998] for cratonic areas and Garnet Lherzolite [*Jordan*, 1979] outside the cratons. The former composition might underestimate the effect of strong depletion (Mg#∼92 or more) characterizing some Archean cratons (e,g,. the Slave craton) or part of them, which translates in an underestimation of temperature (∼100–150°C) and in a consequent overestimation of Te_r (of ∼20% of its value). Furthermore, the anelasticity model (Q_5) that gives intermediate temperature estimates [*Cammarano et al.*, 2003] was chosen. Drier conditions in the cratons would lead to an overestimation of temperature up to ∼200°C. In contrast, the effect of water and melt content on seismic velocities could be underestimated in the areas characterized by strongly hydrated mantle, on account of subduction processes (e.g, North America Cordillera) and would enhance the effect of anelasticity. Therefore, in these regions the temperature might have been overestimated few hundred degrees. However, the choice of the anelasticity model is not relevant for the estimation of Te_r. Indeed, as previously discussed, at temperature >900°C, despite the rheological law and parameters used, the lithospheric mantle strength is negligible and, therefore, does not have any effect on Te_r.

[32] In summary, the relative contributions of uncertainties from thermal and rheological models to Te_r estimates are difficult to quantify because they may compensate each other. Uncertainties in the tomography model are more difficult to constrain and likely strongly affect the Te_r estimates, since they arise from different sources (e.g., uneven data coverage, choice of a reference model and crustal correction). Nevertheless, the above discussion provides an overview of the potential sources of discrepancies between our estimates within cratonic areas. Finally, in these regions our models diverge of few tens of km, but such a difference is in many cases within the uncertainties of the estimates of our models (representing less than 20% of their values), suggesting either that uncertainties in model parameters are small or that they compensate each other.

5. Conclusions

[33] For the first time we had the opportunity to compare the effective elastic thickness (*Te*) estimated worldwide for the continental areas using two independent approaches. The rheological approach (Te_r) is based on the strength distribution estimated from thermo-rheological parameters [*Tesauro et al.*, 2012]. The inverse (Te_i) approach is based on a comparison of the spectral coherence between topography and gravity anomalies and the flexural response of an equivalent elastic plate to loading [*Audet and Bürgmann*, 2011].

[34] The two models span a similar range, from 10 to 200 km (Te_i) and from 15 to 180 km (Te_r), respectively. Te_r shows a bimodal distribution with the main peaks around 25 km and between 65 and 80 km, which are typical values of the continental lithosphere having mechanically decoupled and coupled layers, respectively. In contrast, the Te_i estimates do not show strong maxima, but a great proportion of them are similar to the values of the main peaks of Te_r. Results of the Welch's t test show that in about half of the continental areas the two models have equal means (at the 95% significance level). In the other regions Te_i is $>Te_r$ in about 65% of the 15° circular search regions.

[35] We analyze in more details consistency of the two models comparing their values along selected cross-sections and their distributions for different crustal ages and tectonic provinces. Although the models show in some cases a different trend (e.g., in the African metacraton), both have a relatively high percentage of values >70 km for the Archean and Proterozoic Shield and Platform provinces, which are typical values for the strong lithosphere. In addition, we find that the Te_i estimates generally exceed Te_r, in these regions. In the Meso-Cenozoic Orogens, the difference between the two models is generally reduced to 5–10 km and both models are characterized by *Te* lower than <30 km.

[36] Finally we compare the average values for selected tectonic regions with most robust determinations. The two models are more highly correlated where the Te_r averages are >40 km, than

where they are <40 km. In the latter case the Te_i averages are ~1.5 time larger than those of Te_r. However, as stated before, the two data sets have more similar range of values in the orogens, than in the cratons. These results give weight to the argument favoring large, long-term strength of cratons compared to orogens [*Burov*, 2010]. Although the accurate determination of *Te* in cratons is difficult, a more thorough analysis of the differences in *Te*, as well as advances in laboratory experiments of rock deformation, may shed light on the appropriate rheological laws and parameters that satisfy both models.

Acknowledgments

[37] We would like to thank the Editor Thorsten Becker, Tony Lowry and an anonymous reviewer for valuable comments that significantly improved this paper. This study was made under the Alexander von Humboldt Foundation post-doctoral grant and was partly supported by the Miller Institute for Basic Research in Science (UC Berkeley). We also acknowledge the German Research Center for Geosciences (GFZ) and the Netherlands Research Centre for Integrated Solid Earth Science (ISES) for supporting this research.

References

Altenbach, H. (2000), An alternative determination of transverse shear stifnesses for sandwich and laminated plates, *Int. J. Solids Struct.*, *37*, 3503–3520, doi:10.1016/S0020-7683(99)00057-8.

Artemjev, M. E., and M. K. Kaban (1991), Isostatic processes and intracontinental orogenesis, *J. Geodyn.*, *13*, 77–86, doi:10.1016/0264-3707(91)90031-9.

Audet, P., and R. Bürgmann (2011), Dominant role of tectonic inheritance in supercontinent cycles, *Nat. Geosci.*, *4*, 184–187, doi:10.1038/ngeo1080.

Bassin, C., G. Laske, and G. Masters (2000), The current limits of resolution for surface wave tomography in North America, *Eos Trans. AGU*, *81*(48), Fall Meeting Suppl., Abstract S12A-03.

Bürgmann, R., and G. Dresen (2008), Rheology of the lower crust and upper mantle: Evidence from rock mechanics, geodesy and field observations, *Annu. Rev. Earth Planet. Sci.*, *36*, 531–567, doi:10.1146/annurev.earth.36.031207.124326.

Burov, E. B. (2010), The equivalent elastic thickness (T_e), seismicity and the long-term rheology of continental lithosphere: Time to burn-out "crème brûlée"? Insights from large-scale geodynamic modeling, *Tectonophysics*, *484*, 4–26, doi:10.1016/j.tecto.2009.06.013.

Burov, E. B. (2011), Rheology and strength of the lithosphere, *Mar. Pet. Geol.*, *28*, 1402–1443, doi:10.1016/j.marpetgeo.2011.05.008.

Burov, E. B., and M. Diament (1995), The effective elastic thickness of (T_e) continental lithosphere. What does it really means?, *J. Geophys. Res.*, *100*(B3), 3905–3927, doi:10.1029/94JB02770.

Burov, E. B., and M. Diament (1996), Isostasy, equivalent elastic thickness, and inelastic rheology of continents and oceans, *Geology*, *24*(5), 419–422, doi:10.1130/0091-7613(1996)024<0419:IEETAI>2.3.CO;2.

Byerlee, J. D. (1978), Friction of rocks, *Pure Appl. Geophys.*, *116*, 615–626, doi:10.1007/BF00876528.

Cammarano, F., S. Goes, P. Vacher, and D. Giardini (2003), Inferring upper-mantle temperatures from seismic velocities, *Phys. Earth Planet. Inter.*, *138*, 197–222, doi:10.1016/S0031-9201(03)00156-0.

Carter, N. L., and M. C. Tsenn (1987), Flow properties of continental lithosphere, *Tectonophysics*, *136*, 27–63, doi:10.1016/0040-1951(87)90333-7.

Christensen, N. I. (1996), Poisson's ratio and crustal seismology, *J. Geophys. Res.*, *101*(B2), 3139–3156, doi:10.1029/95JB03446.

Christensen, N. I., and W. D. Mooney (1995), Seismic velocity structure and composition of the continental crust: A global view, *J. Geophys. Res.*, *100*, 9761–9788, doi:10.1029/95JB00259.

Clark, M., and L. Royden (2000), Topographic ooze: Building the eastern margin of Tibet by lower crustal flow, *Geology*, *28*, 703–706, doi:10.1130/0091-7613(2000)28<703:TOBTEM>2.0.CO;2.

Cloetingh, S., and E. B. Burov (1996), Thermomechanical structure of European continental lithosphere: Constraints from rheological profiles and EET estimates, *Geophys. J. Int.*, *124*, 695–723, doi:10.1111/j.1365-246X.1996.tb05633.x.

Collins, C. D. N., B. J. Drummond, and M. G. Nicoll (2003), Crustal thickness patterns in the Australian continent, *Spec. Pap. Geol. Soc. Am.*, *372*, 121–128.

Divins, D. L. (2003), Total Sediment Thickness of the World's Oceans & Marginal Seas, 2011, http://www.ngdc.noaa.gov/mgg/sedthick/sedthick.html, Natl. Geophys. Data Cent., Boulder, Colo.

Flück, P., R. D. Hyndman, and C. Lowe (2003), Effective elastic thickness *Te* of the lithosphere in Western Canada, *J. Geophys. Res.*, *108*(B9), 2430, doi:10.1029/2002JB002201.

Forsyth, J. (1985), Subsurface loading and estimates of the flexural rigidity of continental lithosphere, *J. Geophys. Res.*, *90*(B14), 12,623–12,632, doi:10.1029/JB090iB14p12623.

Goes, S., R. Govers, and P. Vacher (2000), Shallow mantle temperatures under Europe from *P* and *S* wave tomography, *J. Geophys. Res.*, *105*(B5), 11,153–11,169, doi:10.1029/1999JB900300.

Goetze, C., and B. Evans (1979), Stress and temperature in the bending lithosphere as constrained by experimental rock mechanics, *Geophys. J. R. Astron. Soc.*, *59*, 463–478, doi:10.1111/j.1365-246X.1979.tb02567.x.

Hieronymus, C., and S. Goes (2010), Complex cratonic seismic structure from thermal models of the lithosphere: Effects of variations in deep radiogenic heating, *Geophys. J. Int.*, *180*, 999–1012, doi:10.1111/j.1365-246X.2009.04478.x.

Hirth, G., and D. L. Kohlstedt (1996), Water in oceanic upper mantle: Implications for rheology, melt extraction and the evolution of the lithosphere, *Earth Planet. Sci. Lett.*, *144*, 93–108, doi:10.1016/0012-821X(96)00154-9.

Hyndman, R. D., C. A. Currie, and S. P. Mazzotti (2005), Subduction zone backarcs, mobile belts, and orogenic heat, *GSA Today*, *15*, 4–10.

Jackson, J. (2002), Strength of the continental lithosphere: Time to abandon the jelly sandwich?, *GSA Today*, *9*, 4–10, doi:10.1130/1052-5173(2002)012<0004:SOTCLT>2.0.CO;2.

Jordan, T. H. (1978), Composition and development of the continental lithosphere, *Nature*, *274*, 544–548, doi:10.1038/274544a0.

Jordan, T. H. (1979), Mineralogies, densities and seismic velocities of garnet lehrzolites and their geophysical implications, in *The Mantle Sample: Inclusion in Kimberlites and*

Other Volcanics, edited by F. R. Boyd and H. O. A. Meyer, pp. 1–14, AGU, Washington, D. C., doi:10.1029/SP016p0001.

Kirby, J. F., and C. J. Swain (2009), A reassessment of spectral *Te* estimation in continental interiors: The case of North America, *J. Geophys. Res.*, *114*, B08401, doi:10.1029/2009JB006356.

Kruse, S. E., and L. H. Royden (1994), Bending and unbending of an elastic lithosphere: The Cenozoic history of the Apennine and Dinaride foredeep basins, *Tectonics*, *13*, 278–302, doi:10.1029/93TC01935.

Lee, C.-T. A. (2003), Compositional variation of density and seismic velocities in natural peridotites at STP conditions: Implications for seismic imaging of compositional heterogeneities in the upper mantle, *J. Geophys. Res.*, *108*(B9), 2441, doi:10.1029/2003JB002413.

Lewis, B. T. R., and L. M. Dorman (1970), Experimental isostasy, 2. An isostatic model for the U.S.A. derived from gravity and topographic data, *J. Geophys. Res.*, *75*, 3367–3386, doi:10.1029/JB075i017p03367.

Lowry, A. R., and M. Pérez-Gussinyé (2011), The role of crustal quartz in controlling Cordilleran deformation, *Nature*, *471*, 353–357, doi:10.1038/nature09912.

Lowry, A. R., and R. B. Smith (1995), Strength and rheology of the western U.S. Cordillera, *J. Geophys. Res.*, *100*, 17,947–17,963, doi:10.1029/95JB00747.

McDonough, W. F., and R. L. Rudnick (1998), Mineralogy and composition of the upper mantle, in *Ultrahigh Pressure Mineralogy: Physics and Chemistry of the Earth's Deep Interior*, *Rev. Mineral.*, vol. 37, edited by R. J. Hemley, pp. 139–164, Mineral. Soc. of Am., Washington, D. C.

McKenzie, D. (2003), Estimating T_e in the presence of internal loads, *J. Geophys. Res.*, *108*(B9), 2438, doi:10.1029/2002JB001766.

McKenzie, D. P., and D. Fairhead (1997), Estimates of the effective elastic thickness of the continental lithosphere from Bouguer and free-air gravity anomalies, *J. Geophys. Res.*, *102*, 27,523–27,552, doi:10.1029/97JB02481.

Mooney, W. D. (2009), Crust and lithospheric structure-Global crustal structure, in *Treatise on Geophysics*, vol. 1, *Seismology and the Structure of the Earth*, edited by B. Romanowicz and A. Dziewonski, chap. 11, pp. 361–417, Elsevier, Boston, Mass.

Mooney, W. D., and M. K. Kaban (2010), The North American upper mantle: Density, composition, and evolution, *J. Geophys. Res.*, *115*, B12424, doi:10.1029/2010JB000866.

Ouimet, W. B., and K. L. Cook (2010), Building the central Andes through axial lower crustal flow, *Tectonics*, *29*, TC3010, doi:10.1029/2009TC002460.

Pavlis, N. K., S. A. Holmes, S. C. Kenyon, and J. K. Factor (2008), An Earth gravitational model to degree 2160: EGM2008, paper presented at EGU General Assembly, Eur. Geosci. Union, Vienna.

Pérez-Gussinyé, M., and A. B. Watts (2005), The long-term strength of Europe and its implications for plate-forming processes, *Nature*, *436*, 381–384, doi:10.1038/nature03854.

Pérez-Gussinyé, M., A. R. Lowry, and A. B. Watts (2007), Effective elastic thickness of South America and its implications for intracontinental deformation, *Geochem. Geophys. Geosyst.*, *8*, Q05009, doi:10.1029/2006GC001511.

Pérez-Gussinyé, M., M. Metois, M. Fernández, J. Vergés, J. Fullea, and A. R. Lowry (2009), Effective elastic thickness of Africa and its relationship to other proxies for lithospheric structure and surface tectonics, *Earth Planet. Sci. Lett.*, *287*, 152–167, doi:10.1016/j.epsl.2009.08.004.

Prezzi, C. B. (1999), Diacronismo en la deformación Mio-Pliocena de la Puna Argentina: Un modelo flexural, *Actas Congr. Geol. Argent.*, *14*, 197–200.

Ranalli, G. (1994), Nonlinear flexure and equivalent mechanical thickness of the lithosphere, *Tectonophysics*, *240*, 107–114.

Ritsema, J., H. J. van Heijst, and J. H. Woodhouse (2004), Global transition zone tomography, *J. Geophys. Res.*, *109*, B02302, doi:10.1029/2003JB002610.

Shapiro, N. M., and M. H. Ritzwoller (2004), Thermodynamic constraints on seismic inversions, *Geophys. J. Int.*, *157*, 1175–1188, doi:10.1111/j.1365-246X.2004.02254.x.

Simons, F. J., R. D. van der Hilst, and M. T. Zuber (2003), Spatiospectral localization of isostatic coherence anisotropy in Australia and its relation to seismic anisotropy: Implications for lithospheric deformation, *J. Geophys. Res.*, *108*(B5), 2250, doi:10.1029/2001JB000704.

Smith, W. H. F., and D. T. Sandwell (1997), Global sea floor topography from satellite altimetry and ship depth soundings, *Science*, *277*, 1956–1962, doi:10.1126/science.277.5334.1956.

Swain, C. J., and J. F. Kirby (2006), An effective elastic thickness map of Australia from wavelet transforms of gravity and topography using Forsyth's method, *Geophys. Res. Lett.*, *33*, L02314, doi:10.1029/2005GL025090.

Tassara, A., C. Swain, R. Hackney, and J. Kirby (2007), Elastic thickness structure of South America estimated using wavelets and satellite-derived gravity data, *Earth Planet. Sci. Lett.*, *253*, 17–36, doi:10.1016/j.epsl.2006.10.008.

Teng, J. W. (1991), Geophysical fields and hydrocarbon prospects of the Tarim Basin, *Acad. Sin.*, *2*, 24–40.

Tesauro, M., M. K. Kaban, and S. A. P. L. Cloetingh (2008), EuCRUST-07: A new reference model for the European crust, *Geophys. Res. Lett.*, *35*, L05313, doi:10.1029/2007GL032244.

Tesauro, M., M. K. Kaban, and S. A. P. L. Cloetingh (2009), How rigid is Europe's lithosphere?, *Geophys. Res. Lett.*, *36*, L16303, doi:10.1029/2009GL039229.

Tesauro, M., M. K. Kaban, and S. A. P. L. Cloetingh (2010), Thermal and rheological model of the European lithosphere, in *New Frontiers in Integrated Solid Earth Sciences*, edited by S. A. P. L. Cloetingh and J. F. W. Negendank, pp. 71–101, Springer, Berlin.

Tesauro, M., E. Burov, M. K. Kaban, and S. A. P. L. Cloetingh (2011), Ductile crustal flow in Europe's lithosphere, *Earth Planet. Sci. Lett.*, *312*, 254–265, doi:10.1016/j.epsl.2011.09.055.

Tesauro, M., M. K. Kaban, and S. A. P. L. Cloetingh (2012), Global strength and elastic thickness of the lithosphere, *Global Planet. Change*, *90–91*, 51–57, doi:10.1016/j.gloplacha.2011.12.003.

Wang, Y., and J. C. Mareshal (1999), Elastic thickness of the lithosphere in the Central Canadian Shield, *Geophys. Res. Lett.*, *26*(19), 3033–3036, doi:10.1029/1999GL010806.

Watts, A. B. (2001), *Isostasy and Flexure of the Lithosphere*, 458 pp., Cambridge Univ. Press, Cambridge, U. K.

Watts, A. B., and E. Burov (2003), Lithospheric strength and its relationship to the elastic and seismogenic layer thickness, *Earth Planet. Sci. Lett.*, *213*, 113–131, doi:10.1016/S0012-821X(03)00289-9.

Watts, A. B., S. H. Lamb, J. D. Fairhead, and J. F. Dewey (1995), Lithospheric flexure and bending of the Central Andes, *Earth Planet. Sci. Lett.*, *134*, 9–21, doi:10.1016/0012-821X(95)00095-T.

Whitehouse, P., K. Latychev, G. A. Milne, J. X. Mitrovica, and R. Kendall (2006), Impact of 3-D Earth structure on Fennoscandian glacial isostatic adjustment: Implications for space-geodetic

estimates of present-day crustal deformations, *Geophys. Res. Lett.*, *33*, L13502, doi:10.1029/2006GL026568.

Wilks, K. R., and N. L. Carter (1990), Rheology of some continental lower crustal rocks, *Tectonophysics*, *182*, 57–77, doi:10.1016/0040-1951(90)90342-6.

Yang, Y., M. Liu, and S. Stein (2003), A 3-D geodynamic model of lateral crustal flow during Andean mountain building, *Geophys. Res. Lett.*, *30*(21), 2093, doi:10.1029/2003GL018308.

Zhong, S., and A. B. Watts (2010), Constraints on lithosphere rheology from observations of volcano-induced deformation, Abstract T53C-2152 presented at 2010 Fall Meeting, AGU, San Francisco, Calif., 13–17, Dec.